Design, motivation, and on-sky tests of an efficient fiber coupling unit for 1-meter class telescopes.

Michael Bottom,[a] Philip S. Muirhead,[b] Jonathan J. Swift,[a] Ming Zhao,[c] Paul Gardner,[a] Peter P. Plavchan,[a,h,i] Reed L. Riddle,[a] Erich Herzig,[d] John Asher Johnson,[e] Jason T. Wright,[c] Nate McCrady[f] and Robert A. Wittenmyer[g]

[a]California Institute of Technology, 1200 East California Blvd, Pasadena, CA 91125, USA
[b]Boston University, 725 Commonwealth Ave, Boston, MA 02215, USA
[c]The Pennsylvania State University, 525 Davey Lab, University Park, PA 16803, USA
[d]The Thacher School, 5025 Thacher Rd, Ojai, CA 93023
[e]Harvard College Observatory, 60 Garden Street, Cambridge, MA 02138, USA
[f]University of Montana, 32 Campus Drive, No. 1080, Missoula, MT 59812, USA
[g]School of Physics, UNSW Australia, Sydney 2052, Australia
[h]Missouri State University, 901 S National Ave, Springfield, MO 65897, USA
[i]NASA Exoplanet Science Institute, 770 South Wilson Avenue, Pasadena, CA 91125, USA

ABSTRACT

We present the science motivation, design, and on-sky test data of a high-throughput fiber coupling unit suitable for automated 1-meter class telescopes. The optical and mechanical design of the fiber coupling is detailed and we describe a flexible controller software designed specifically for this unit. The system performance is characterized with a set of numerical simulations, and we present on-sky results that validate the performance of the controller and the expected throughput of the fiber coupling. This unit was designed specifically for the MINERVA array, a robotic observatory consisting of multiple 0.7 m telescopes linked to a single high-resolution stabilized spectrograph for the purpose of exoplanet discovery using high-cadence radial velocimetry. However, this unit could easily be used for general astronomical purposes requiring fiber coupling or precise guiding.

Keywords: exoplanets, fiber, fiber feed, coupling, radial velocity, guiding, small telescope

1. INTRODUCTION AND SCIENCE MOTIVATION

More than 400 extrasolar planets have been discovered via the radial velocity method ,[1] where the tiny shift in stellar spectral lines caused by an orbiting planet are measured with high resolution spectroscopy. A typical shift caused by a planet like Earth around a Sun-like star is only 10 cm/s, corresponding to a line shift of a few dozen silicon atoms on a high-resolution optical spectrograph .[2] This leads to extreme requirements for thermal and mechanical stability of the spectrograph, which become more difficult to achieve for larger telescope primary mirror, as the spectrograph collimator diameter must grow proportionally to keep the resolution constant.[3] On the other hand, a larger mirror is beneficial for attaining the necessarily high signal-to-noise ratio in reasonable amounts of observing time. Finally, in order for a planet to be detected, measurements must be made with adequate orbital phase coverage, which can stretch from days to years depending on the orbital distance.

In view of these challenges, we are developing a fully robotic observatory to detect habitable-zone super-Earths around nearby stars, called the "Minature Exoplanet Radial Velocity Array" (MINERVA). Rather than use a single dish/single spectrograph design, the observatory uses multiple smaller telescopes fiber-feeding a single spectrograph. The smaller dish size means that a high resolution can be achieved with a relatively compact (and hence easier to stabilize) spectrograph, with the penalty of increased detector size. Furthermore, the multiple spectra traced on the detector lead to better systematic error control.

Further author information: (Send correspondence to Michael Bottom)
E-mail: mbottom@caltech.edu

Ground-based and Airborne Instrumentation for Astronomy V, edited by Suzanne K. Ramsay, Ian S. McLean, Hideki Takami, Proc. of SPIE Vol. 9147, 91472E · © 2014 SPIE · CCC code: 0277-786X/14/$18 · doi: 10.1117/12.2055605

A critical component of this system is the fiber acquisition unit (FAU), where starlight is coupled from the telescope to the spectrograph. Such a system must be robust, efficient, and automated in order to reduce observing overhead and maximize signal.

2. SYSTEM OVERVIEW

MINERVA consists of four PlaneWave* CDK-700 telescopes with four imaging cameras, four fiber acquisition units (FAUs) and a single high resolution spectrograph. Each telescope will have one fiber coupler and one wide-field imaging camera. The telescopes use a corrected Dall-Kirkham optical design with a tertiary mirror providing access to two Nasmyth ports.

3. DESIGN

The coupling system consists of a fiber acquisition unit (FAU) and control software to interface analysis and correction with the telescope pointing system. We first discuss the optical design and its implementation.

3.1 Optomechanical design

The FAU has three accessible optical paths. In the primary path, the telescope beam is fed directly into the fiber at the native f/6.6 of the telescope. Separately, there is an optical path which relays a portion of the light to a guiding camera via a pellicle. Finally, there is a set of relay lenses and a corner retroreflector. If the fiber is illuminated from the exit end near the spectrograph, the input end of the fiber tip will be imaged on the guide camera. The corner retroreflector guarantees that misalignments of the optics do not affect the image position; this allows determination of the pixel position on the guider that corresponds to the fiber tip, and hence a setpoint for guiding.

The fibers we use are 50 μm Ceramoptec octagonal fibers, which corresponds to a sky diameter of 2.3 arc seconds. The median seeing at Mt. Hopkins observatory location is about a factor of two better than this, ensuring that minimal flux is lost at the wings of the seeing disk.

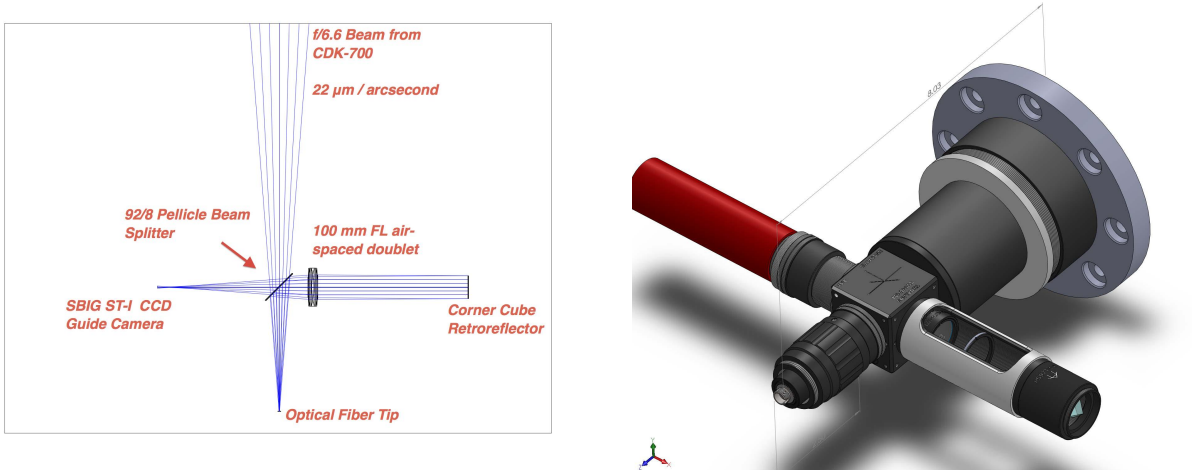

Figure 1: Left: Optical layout of the fiber acuisition unit. The primary beam path (top to bottom) couples light from the telescope into the fiber. The second path (top to left) images the star onto a guide camera. The third path (bottom to right to left) images the fiber tip onto the detector. Right: mechanical drawing of the FAU; fiber tip to base is about 8 inches long.

*www.planewave.com

3.2 Controller design

While the CDK-700 telescope has quite good open-loop tracking (accurate to a couple of arc-seconds over a ten minute period), this is not good enough for our purposes, as typical integration times are from 10-20 minutes and require keeping the star centered on a 2.3" diameter fiber tip. Therefore, we have implemented a modified positional PID-type controller to correct for drifts and other inaccuracies. The controller input is the star position on the camera, and the output is alt-az offsets to the telescope mount. It typically sends corrections once every few seconds. The geometry of the alt-az telescope allows us to perform a "one-time" calibration of the camera field rotation if the telescope's derotator is turned off, which is ideal for high-cadence observing.

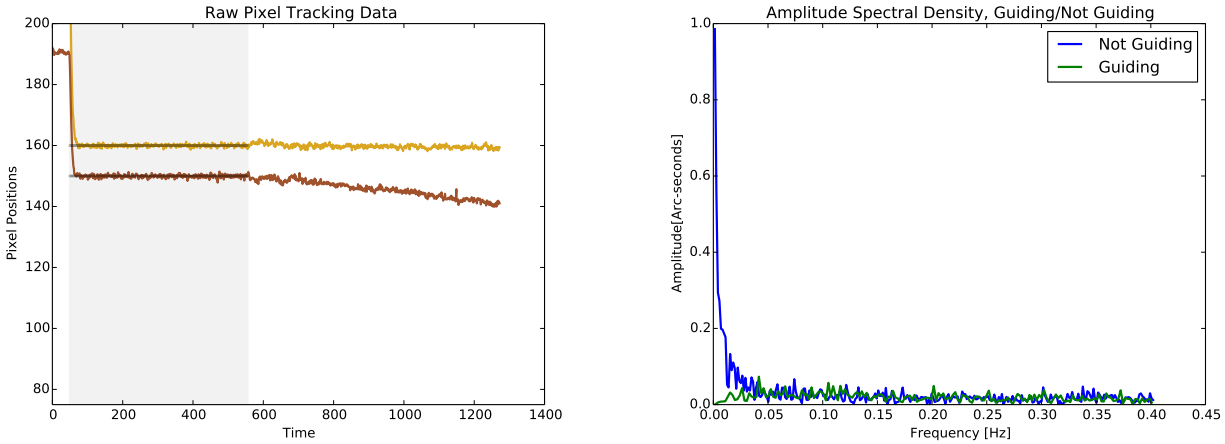

Figure 2: (Left) Raw pixel tracking data with the closed loop guiding on (shaded region) and off. The two curves correspond to the x and y pixel positions on the guider CCD. The pitch is 0.33 arc seconds per pixel. (Right) The amplitude spectral density of the guider error is smaller at essentially all frequencies when guiding, especially low frequencies corresponding to long-term drifts. The intersection of the green (guiding) curve with 0 at 0 Hz indicates there is no systematic error.

Currently, the controller operates near the optimal level, showing an rms pointing precision of about 0.2 arc seconds, dominated by uncertainties in the measurement from seeing variations. Simulations of the required pointing accuracy indicate that very low coupling penalties are incurred for a pointing accuracy of 0.2" rms at any seeing from 0.5 - 2.5 "; typically from 0-5%. It is thus unlikely that the control system is contributing to any major loss of throughput in the system. Results from pointing tests are shown in Figure 2. The most convincing evidence that the controller is not adding significant noise to the pointing system is from examining the amplitude spectral density of the pointing errors; the error is comparable or lower at all sensed frequencies when the telescope is guiding.

4. EXPECTED PERFORMANCE

The throughput of the fiber system is defined as the ratio of output light from the fiber to incident light on the FAU. The throughput may be expressed in the following way:

$$\text{Throughput} = \text{Pellicle Transmission} * \text{Fiber Transmission} \quad (1)$$

$$= P\eta_{\mathrm{R_{in}}}\eta_{\mathrm{in}}\eta_{\mathrm{thru}}\eta_{\mathrm{R_{out}}} \quad (2)$$

where η_{in} is the input coupling efficiency of the fiber tip, η_{thru} is the throughput of the fiber (which depends on the fiber length and wavelength of light), and $\eta_{\mathrm{R_{out}}}$ is the output transmission of the other fiber tip. Implicit in the above equation is the wavelength dependence on all these quantities, and in all that follows, the flux should be interpreted as an integral over the V-band.

We will consider these terms one by one.

4.1 Pellicle

The pellicle is a Thorlabs BP108 92% / 8% transmission/reflection model. (While these values are strongly polarization dependent, the expected polarization level of the light is low.) Assuming the unpolarized transmission curve we calculate the transmission over the Johnson V-band and find an expected transmission of 90.12 %.

$$\frac{\int P_T(\lambda)V(\lambda)d\lambda}{\int V(\lambda)d\lambda} = 90.12\% \tag{3}$$

4.2 Fiber losses: $\eta_{\mathrm{R_{in}}}$, η_{in}, η_{thru}, $\eta_{\mathrm{R_{out}}}$

4.2.1 Reflection losses: η_{Rin}, $\eta_{\mathrm{R_{out}}}$

The input coupling efficiency is dependent on two factors, the reflection from the fiber tip and the coupling into the fiber tip. The reflection loss can be determined from the Fresnel equation(s) for $s-$ and $p-$ polarized light. Both of these expressions can be approximated by

$$R = \left(\frac{n_1 - n_2}{n_1 + n_2}\right)^2 \tag{4}$$

which gives a reflection loss of **5.3%** on input assuming an index of refraction of silicon of 1.6. Using the exact Fresnel equations does not change the answer very much (5.30% and 5.34%, respectively) even assuming all the rays are propagating at the most extreme angle of the telescope's f/#.

The same result holds on output, as the expression (the simplified one) is the same on interchange from 1→2.

4.2.2 Fiber input losses, η_{in}

The input efficiency depends on the coupling integral between the fiber and the image of the star[†]:

$$C = \frac{\int_{-\infty}^{\infty} \mathrm{Fiber}(\theta_\mathrm{x}, \theta_\mathrm{y}) \times \mathrm{Star}(\theta_\mathrm{x}, \theta_\mathrm{y}) \mathrm{d}\theta_\mathrm{x} \mathrm{d}\theta_\mathrm{y}}{\int_{-\infty}^{\infty} \mathrm{Star}(\theta_\mathrm{x}, \theta_\mathrm{y}) \mathrm{d}\theta_\mathrm{x} \mathrm{d}\theta_\mathrm{y}} \tag{5}$$

The full integral needs to be performed in 2 dimensions. The input seeing is assumed to be a symmetric gaussian with a fwhm equal to the seeing; the fiber is assumed to be an octagon with width equal to the fiber image on the sky. Full transmission is assumed inside the octagon; no transmission is assumed outside.

It can be seen in Figure 3 that losses depend heavily on the seeing, and in Pasadena (where the tests were performed), we are operating well below optimal conditions.

It is also possible to calculate how the geometric coupling efficiency depends on pointing accuracy. To do this, we run a Monte Carlo simulation of the coupling efficiency by treating the centroid of the seeing profile as a random variable with zero mean error and a standard deviation equal to the pointing precision, shown as well in Figure 3. It is interesting to note that for good pointing (0.1"-0.2"), the most severe losses occur at *good* but not *excellent* seeing. The reason for this is that at excellent seeing (0-0.5"), the starlight is smaller than and completely contained within the fiber tip and minor pointing errors do not change this. For good seeing (0.8-1.7"), the same pointing errors cause significant portions of the seeing disk to miss the fiber tip. For poor seeing (1.7+"), the seeing disk is already leaking out of the sides of the fiber tip, and small pointing errors only have a modest additional effect.

[†]this is a simplification; the full equation involves the mode field diameter of the each fiber mode and the electric field of the input star light

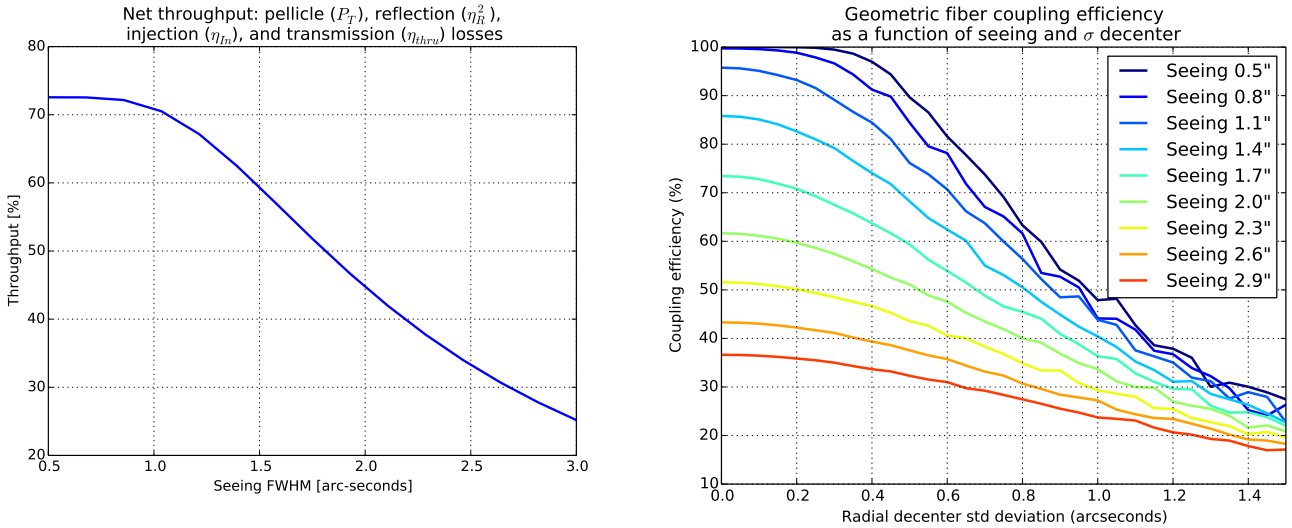

Figure 3: Left: Theoretical throughput including pellicle transmission (P_T), reflection ($\eta_{\rm R}$), geometric fiber injection ($\eta_{\rm in}$), and fiber transmission ($\eta_{\rm thru}$) loss, for a range of seeing values. Right: Numerical simulation of geometric injection efficiency for a range of pointing accuracies. The different lines correspond to different values of seeing.

4.3 Summary of expected transmission

A summary of the expected transmission for each optical element is shown below. The weakness in these values is that except for the pellicle, the transmissions were all derived from data sheets or calculated from numerical simulations. Therefore, the uncertainty in the final number are expected to be at the 10-20% level.

Item	Label	Transmission	Source	Comment
Pellicle	P	0.9	Thorlabs data, measured	Integrated over V-band
Input Reflection	$\eta_{\rm R_{in}}$	0.947	Calculated	Fresnel equation, unpolarized
Input Coupling	$\eta_{\rm In}$	0.45–0.55	Numerical simulations	Coupling integral, seeing=2–2.5”
Fiber Transmission	$\eta_{\rm thru}$	0.90	Optran Data sheet	40 m fiber, calculated over V-band
Output Reflection	$\eta_{\rm R_{out}}$	0.947	Calculated	Fresnel equation, unpolarized
Product		0.34–0.45		

5. MEASURED PERFORMANCE

To assess the performance of the fiber acquisition unit, we used two CCD cameras to synchronously measure the reflected starlight and light transmitted out of the end of the fiber. The two cameras are identical SBIG ST-i monochrome models, which were both fully characterized to assess gain and dark current differences. One of the cameras was the actual camera used for guiding; the other was attached to the end of the fiber with an identical V-band filter. A typical output image from the test is shown below in Figure 4.

The fundamental quantity measured from these two cameras is ADU's, which can be related to the input flux and other optical constants:

$$\text{Guidecam[ADU]} = \frac{\text{I[photons/s]} \cdot \text{P}_\text{R} \cdot \text{QE[e}^-\text{/photon]}}{\text{Gain}_\text{guider}\text{[e}^-\text{/ADU]}} \cdot \text{t}_\text{exp,guider}\text{[s]} \tag{6}$$

And the integrated counts on the fiber are:

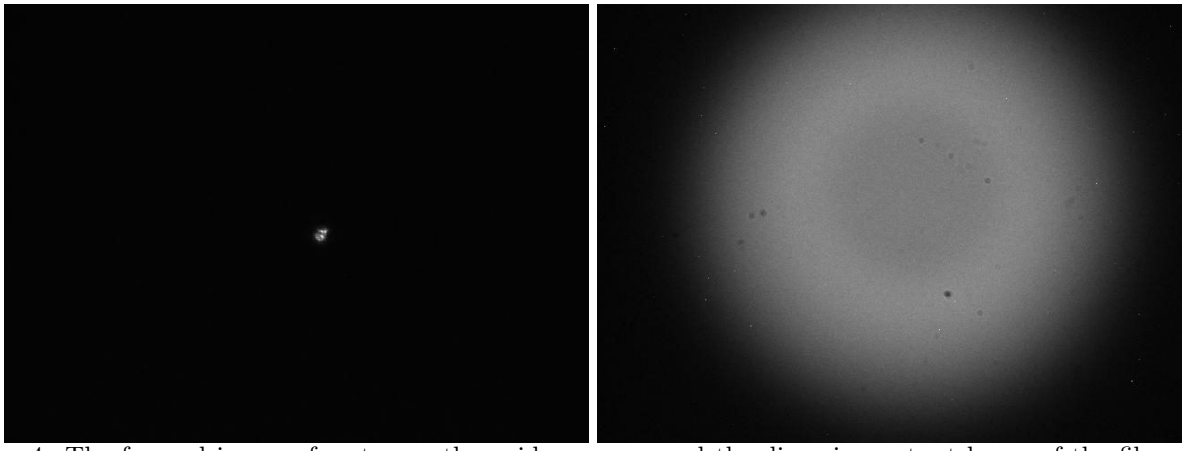

Figure 4: The focused image of a star on the guide camera, and the diverging output beam of the fiber. The region of relatively reduced flux in the center of the fiber image is due to the effects of focal ratio degradation.

$$\text{Fibercam[ADU]} = \frac{\text{I[photons/s]} \cdot \text{P}_\text{T} \cdot \eta_\text{R}\ \eta_\text{In}\ \eta_\text{thru}\ \eta_\text{R} \cdot \text{QE[e}^-\text{/photon]}}{\text{Gain}_\text{Fibercam}[\text{e}^-\text{/ADU}]} \cdot \text{t}_\text{exp,fiber}[\text{s}] \tag{7}$$

Where P_R, P_T is the pellicle reflectance and transmission. Assuming the QE is the same for both cameras (which is reasonable, as they use the same sensor), we can take the ratio of the two expressions above to find

$$\frac{\text{Fibercam[ADU]}}{\text{Guidecam[ADU]}} = \frac{\text{P}_\text{T}}{\text{P}_\text{R}} \frac{\text{Gain}_\text{guider}}{\text{Gain}_\text{Fibercam}} \frac{\text{t}_\text{exp,fiber}}{\text{t}_\text{exp,guider}} \times \eta_\text{R}^2 \eta_\text{In} \eta_\text{thru} \tag{8}$$

or more usefully

$$\text{FAU efficiency} = \eta_\text{R}^2 \eta_\text{In} \eta_\text{thru} = \frac{\text{Fibercam[ADU]}}{\text{Guidecam[ADU]}} \frac{\text{P}_\text{R}}{\text{P}_\text{T}} \frac{\text{Gain}_\text{Fibercam}}{\text{Gain}_\text{guider}} \frac{\text{t}_\text{exp,guider}}{\text{t}_\text{exp,fiber}} \tag{9}$$

$$\text{FAU Transmittance} = \text{P}_\text{T} \eta_\text{R}^2 \eta_\text{In} \eta_\text{thru} = \frac{\text{Fibercam[ADU]}}{\text{Guidecam[ADU]}} \text{P}_\text{R} \frac{\text{Gain}_\text{Fibercam}}{\text{Gain}_\text{guider}} \frac{\text{t}_\text{exp,guider}}{\text{t}_\text{exp,fiber}} \tag{10}$$

We performed multiple tests in both open and closed loop to assess the performance of the optical system and control system. The tests were performed over a number of stars of differing magnitudes and spectral types. We found that we typically measure throughputs of 35-45%, in line with the expectations from Figure 3 and consistent with independent seeing measurements performed using a wide-field camera on the opposite Nasmyth port of the telescope. An example of such a measurement can be seen in Figure 5.

6. CONCLUSION

We have presented the design, numerical simulations, and throughput measurements of a fiber coupling unit suitable for small telescopes. The instrument has a simple and robust design and has proven to be reliable, with performance in line with expectations within the precision of the measurements. Further tests after deployment at Mt. Hopkins should validate the performance in more optimal seeing conditions. The final version(s) of this instrument will be deployed later this year, and will incorporate minor modifications such as a customized pellicle for slightly higher transmission (98% vs 92 %) and a slightly different fiber.

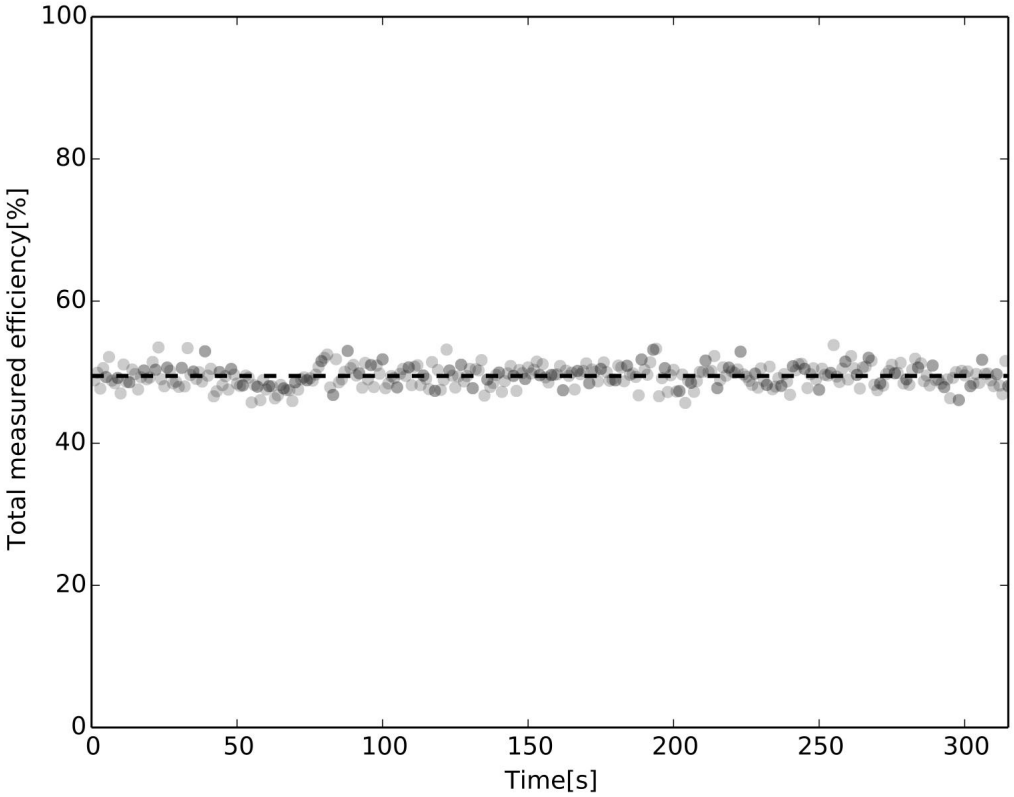

Figure 5: A throughput measurement in typical Pasadena seeing conditions of ∼2". The efficiency is about 50% (45% throughput), in line with the expectations of Figure 3. The statistical deviation about the mean is 1.5% (absolute), which is smaller than our systematic error.

6.1 Acknowledgments

MB is supported by a NASA Space Technology Research Fellowship, and would like to acknowledge Kevin Ivarsen of PlaneWave Instruments for valuable assistance and discussions. JAJ is grateful for the generous grant support provided by the Alfred P. Sloan and David and Lucile Packard foundations. PPP acknowledges support from the JPL Research and Technology Development program. J.T.W. is affiliated with the Center for Exoplanets and Habitable Worlds, which is supported by the Pennsylvania State University, the Eberly College of Science, and the Pennsylvania Space Grant Consortium; and by the Penn State Astrobiology Research Center, part of the NASA Astrobiology Institute (grant NNA09DA76A). RW acknowledges support from the Australian Research Council LIEF grant LE140100050 and Major Research Equipment funding from UNSW.

REFERENCES

[1] J. T. Wright, O. Fakhouri, G. W. Marcy, E. Han, Y. Feng, J. A. Johnson, A. W. Howard, D. A. Fischer, J. A. Valenti, J. Anderson, and N. Piskunov, "The Exoplanet Orbit Database," *Publications of the Astronomical Society of the Pacific* **123**, pp. 412–422, Apr. 2011.

[2] M. Perryman, *The Exoplanet Handbook*, Cambridge University Press, 2011.

[3] D. J. Schroeder, *Astronomical Optics; 2nd ed.*, Elsevier, Burlington, MA, 1999.